Autoresonant four-wave mixing in optical fibers

O. Yaakobi and L. Friedland
Racah Institute of Physics, The Hebrew University, Jerusalem 91904, Israel
(Received 3 May 2010; published 30 August 2010)

A theory of autoresonant four-wave mixing in tapered fibers is developed in application to optical parametric amplification (OPA). In autoresonance, the interacting waves (two pump waves, a signal, and an idler) stay phase-locked continuously despite variation of system parameters (spatial tapering). This spatially extended phase-locking allows complete pump depletion in the system and uniform amplification spectrum in a wide frequency band. Different aspects of autoresonant OPA are described including the automatic initial phase-locking, conditions for autoresonant transition, stability, and spatial range of the autoresonant interaction.

DOI: 10.1103/PhysRevA.82.023820 PACS number(s): 42.81.−i, 42.65.Sf, 42.81.Qb, 42.65.Ky

I. INTRODUCTION

Resonant wave interactions (RWI) are common to many fields of physics and engineering. These interactions involve several waves propagating in a background medium, which defines both the dispersion properties of each wave and alternatives of coupling to other waves. Frequently a single wave in a weakly nonlinear medium can be described by its rapidly varying phase φ and slow envelope A. Nonlinearities play a major role in the RWI and may significantly affect the evolution of the waves. For example, a typical lowest order nonlinearity of a single wave yields a third order (in terms of A) self-modulation term in the envelope equation. If several different waves propagate in the medium, then, in addition to the self-modulation of each wave, there appear important third order cross-modulation terms in the envelope equations, as well as wave mixing terms involving products of the wave envelopes multiplied by $\exp(i\Psi)$, Ψ being the phase mismatch between the waves. These mixing terms are only important when Ψ is nearly stationary meaning a near resonance condition on the frequencies and wave vectors of the interacting waves. While the lowest nonlinear order of self- and cross-modulation terms in the envelope equations is typically three, the order of the wave mixing terms may be different. It defines the number of waves involved in the mixing process and can be used in classifying RWI of distinct (nondegenerate) waves. For example, RWI of two waves involves a linear (in terms of the wave envelope) mixing term and the phase mismatch of form $\Psi = \varphi_1 \pm \varphi_2$. Frequently, this wave interaction process in a nonuniform media is called mode conversion [1]. RWI of three waves has mixing terms involving products of two envelopes. This type of mixing is characteristic of many important applications in fluids, plasmas, acoustics, etc. (see [2] and references therein). The phase mismatch in this case involves phases of three waves $\Psi = \varphi_1 \pm \varphi_2 \pm \varphi_3$, while the three-wave resonance condition is frequently easier to satisfy, than the two-wave resonance in a variety of applications. Finally, if the three-wave resonance cannot be satisfied, a higher order, four-wave mixing, with the product of three envelopes and $\Psi = \varphi_1 \pm \varphi_2 \pm \varphi_3 \pm \varphi_4$ in the mixing term in the envelope equations may become important. This phenomenon has many applications in optics, particularly in fiber optics [3,4].

Satisfaction of a resonance (phase matching) condition is of primary importance in all RWI described above. Therefore, it seems that efficient applications of wave mixing in an extended domain require a high degree of uniformity of the background medium. For example, in the last decades there has been an extensive effort of studying these processes in axially uniform optical fibers (see, for example, [3,4] and references therein). Nevertheless, a different RWI scheme, based on the idea of autoresonance, uses the nonuniformity (or time dependence) of the medium as an advantage. Autoresonance is a unique property of many driven nonlinear systems to stay in resonance (phase-lock) with driving oscillations even if the parameters of the system vary in space and/or time. This phenomenon was first realized in relativistic particle accelerators [5,6], but in the last 20 years it was also applied to excitation and control of nonlinear coherent structures in many other fields ranging from nonlinear dynamics and nonlinear waves to fluids, plasmas, and atomic physics [7,8]. Some applications focused on autoresonant two- and three-wave mixing [9–12] with plasma applications in mind. Recently, autoresonant interaction was also studied in optics in spatially chirped nonlinear directional coupler experiments (a two-wave mixing process [13]). A unique feature of autoresonance is the need of a nonuniformity in the system, but, at the same time, its insensitivity to the exact form of the nonuniformity, as long as the latter is sufficiently adiabatic. It is this insensitivity, which makes autoresonant wave-mixing process attractive. Nevertheless, the entrance into the autoresonant interaction regime is nontrivial and usually requires starting out and a slow passage through the resonance. If these conditions are not met, the autoresonant phase-locking between the waves is not established or lost. In the present work, for the first time, we analyze a nondegenerate four-wave mixing (FWM) process in application to optical parametric amplification (OPA) in tapered fibers.

The underlying mechanism of OPA is based on resonant interaction between two strong pump waves and a weak signal wave and involves excitation of a fourth (idler) wave. In an axially uniform fiber, the highest amplification of a signal is obtained at some specific signal frequency, which may lead to a complete pump depletion for a certain fiber length. If one deviates from this specific frequency, the gain factor decreases, so that the efficient operation (near complete pump depletion) becomes limited to a relatively small frequency band. Different designs are used in trying to compromise between conflicting requirements of having both efficient and wide frequency

band OPA in uniform fibers [4]. In this paper, we discuss an autoresonant two-pump OPA based on a tapered fiber, enabling a *complete* pump depletion in a predefined frequency domain. Consequently, the resulting amplification is efficient in a *wide* frequency band.

The scope of our presentation will be as follows. In the next section, we proceed from the envelope equations of a nondegenerate four-wave mixing process in a weakly nonuniform fiber and illustrate autoresonant evolution in this system in numerical simulations. In Sec. III, we discuss the initial phase-locking stage in the problem and the necessary conditions for entering the autoresonant evolution by passage through resonance. Analytic autoresonant solutions of the envelope equations, their stability and spectral autoresonant amplification profiles will be also described in Sec. III. Finally, our conclusions are summarized in Sec. IV.

II. ENVELOPE EQUATIONS

A. The model

Our starting point is the set of the envelope equations describing a nondegenerate FWM process in an optical fiber [4]:

$$\frac{dA_l}{dz} = i\gamma\left(|A_l|^2 A_l + 2\sum_{j\neq l=1}^{4}|A_j|^2 A_l + 2A_m A_n A_k^* e^{i\varepsilon\Psi}\right), \tag{1}$$

where $l = 1$–4 and the integers k, l, m, and n are such that if $l = 1$ or 2 (the two pump waves), then $k = 3 - l$, $m = 3$, $n = 4$, and $\varepsilon = 1$. For $l = 3$ or 4 (the signal and the idler), then $k = 7 - l$, $m = 1$, $n = 2$ and $\varepsilon = -1$. We assume a slowly varying propagations "constants" $\beta_l(z)$ for each of the interacting waves and define the phase mismatch $\Psi \equiv \int_0^z \Delta\beta(z')dz'$, where $\Delta\beta(z) = \beta_3 + \beta_4 - \beta_1 - \beta_2$. The three terms in the right hand side of Eq. (1) represent the self- and cross-modulation and the wave mixing, respectively. For simplicity, in our theory we assume that the nonlinearity coefficient γ in Eq. (1) is a constant, i.e., we neglect all frequency and fiber tapering effects (the total change of the core radius of the fiber in our examples will be about 5%), except via the presence of the z dependence of $\Delta\beta(z)$ in the phase mismatch.

Following [4] we define the dimensionless amplitude $a_l = A_l/\sqrt{P_0}$, coordinate $\zeta = \gamma P_0 z$ and phase mismatch $S = \Psi/(\gamma P_0)$, P_0 being the total power of the signal, the pumps and the idler (note that $\sum_{l=1}^{4}|a_l|^2 = 1$). Then Eq. (1) yields

$$\frac{da_l}{d\zeta} = i(2 - |a_l|^2)a_l + 2ia_m a_n a_k^* e^{i\varepsilon S(\zeta)}, \quad l = 1\text{–}4. \tag{2}$$

Next, we introduce the phase-shifted amplitudes $b_l = a_l e^{-i2\zeta}$ for $l = 1$–3 and $b_4 = a_4 e^{i(-2\zeta+S)}$, write $b_l = B_l e^{i\phi_l}$, where $B_l = |b_l|$ and $\phi_l = \arg(b_l)$, and define the phase mismatch $\Phi = \phi_3 + \phi_4 - \phi_1 - \phi_2$. Then Eq. (2) reduces to the following set of real equations:

$$\frac{dB_l}{d\zeta} = -2\varepsilon B_k B_m B_n \sin\Phi, \quad l = 1\text{–}4, \tag{3}$$

$$\frac{d\Phi}{d\zeta} = R + Q\cos\Phi, \tag{4}$$

where $R \equiv \Delta B^2 + \Delta\beta/(\gamma P_0)$, $\Delta B^2 = B_1^2 + B_2^2 - B_3^2 - B_4^2$, and $Q = 2B_1B_2B_3B_4\left(B_3^{-2} + B_4^{-2} - B_1^{-2} - B_2^{-2}\right)$. The amplitude equations (3) yield the Manley-Rowe relations:

$$B_1^2 + B_4^2 = B_{10}^2 + B_{40}^2, \tag{5}$$

$$B_2^2 + B_4^2 = B_{20}^2 + B_{40}^2, \tag{6}$$

$$B_3^2 - B_4^2 = B_{30}^2 - B_{40}^2, \tag{7}$$

where B_{l0} denotes the initial amplitude of the lth wave at $z = 0$. Using these relations we rewrite Eq. (4) as

$$\frac{d\Phi}{d\zeta} = R_0 - 4B_4^2 + Q\cos\Phi, \tag{8}$$

where $R_0 \equiv \Delta B_0^2 + \Delta\beta/(\gamma P_0)$ and $\Delta B_0^2 = B_{10}^2 + B_{20}^2 - B_{30}^2 - B_{40}^2$. Next, assuming for simplicity that $\Delta\beta$ is linear in z, $\Delta\beta = \alpha(\gamma P_0)^2(z - z_0)$, and defining a shifted normalized coordinate $\xi = \Delta B_0^2/\alpha - \gamma P_0 z_0 + \zeta$, we rewrite our system (3) and (8) as

$$\frac{dB_4}{d\xi} = 2B_1B_2B_3\sin\Phi, \tag{9}$$

$$\frac{d\Phi}{d\xi} = \alpha\xi - 4B_4^2 + Q\cos\Phi. \tag{10}$$

The remaining amplitudes, $B_{1,2,3}$, can be expressed via B_4 by using the Manley-Rowe relations. Note that the location of $\xi = 0$ corresponds to the point along the fiber, where $R' = 0$, i.e., $\Delta\beta = -\gamma P_0 \Delta B_0^2$. The autoresonant dynamics illustrated below is confined to the region adjacent to $\xi = 0$.

B. Numerical examples

In the following examples, we will present the dependent variables as functions of the reduced coordinate $|\alpha|\xi$. We will always assume that the direction of propagation of the four waves in the physical space is positive, i.e. the final value z_f of z is larger than the initial value z_{in}. Nevertheless, the spatial chirp rate may be positive or negative, corresponding to the decreasing or increasing fiber radius (of course, one can use the same tapered fiber and launch the waves in the opposite direction for changing the sign of α). Our first example (see Fig. 1) shows the solution of Eqs. (9) and (10) for $\alpha = 0.06$ in the interval $-3 \leqslant |\alpha|\xi \leqslant 5$. Here and throughout the paper we will use initial conditions $B_{10}^2 = B_{20}^2 = 0.495$, $B_{30}^2 = 0.01$, $B_{40} = 0$, and $\Phi_0 = 0$. One can split the evolution of the system in Fig. 1 into three major stages. In the first initial stage ($|\alpha|\xi < -2$) the phase mismatch Φ oscillates around the average value of $\Phi \approx 0$, but is bounded (phase-locked) and its oscillations diminish as we approach $|\alpha|\xi = -2$. Despite this phase-locking, there is no significant transfer of energy from the pumps to the signal and idler at this stage. In the second stage ($-2 < |\alpha|\xi < 4$ in Fig. 1) the phase-locking continues, but involves efficient excitation of the signal and idler leading to pump depletion. The square amplitudes of all four waves evolve linearly in $|\alpha|\xi$ in average, but also include slow oscillating modulations. The same frequency modulations are characteristic of the evolution of Φ. The amplification process continues, until almost complete pump depletion is achieved at $|\alpha|\xi = 4$. This stage will be called autoresonant stage in the following. In the last stage ($|\alpha|\xi > 4$), the signal and

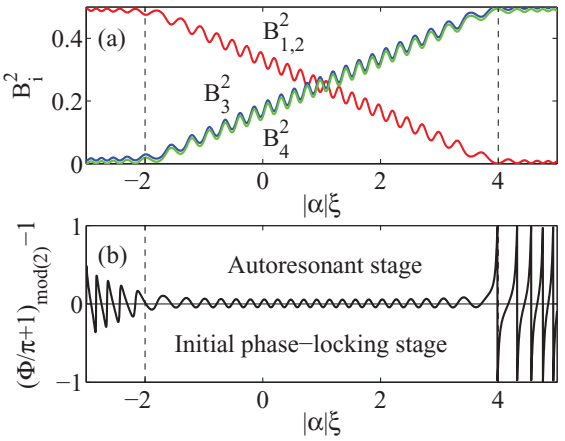

FIG. 1. (Color online) Autoresonant evolution of (a) wave envelopes B_i^2 and (b) phase mismatch Φ in a tapered fiber OPA versus normalized distance $|\alpha|\xi$ along the fiber for positive spatial chirp rate, $\alpha = 0.06$. The equal pumps $B_{1,2}^2$ are shown by the red (decreasing) curve, the signal B_3^2 is shown by the blue (upper increasing) curve and the idler B_4^2 is shown by the green (lower increasing) curve. Note that the curves of the signal and the idler are almost overlapping.

idler waves reach saturation as the pumps are almost fully depleted, the autoresonant phase-locking discontinues, and there is no further significant change in the power partition between the waves. In Fig. 2, we present the numerical solution of Eqs. (9) and (10) for negative $\alpha = -0.06$ in the interval $-3 \leqslant |\alpha|\xi \leqslant 1$. Qualitatively the dynamics is similar to the positive α case. The initial phase-locking stage for $\alpha < 0$ again ends at $|\alpha|\xi = -2$. Nevertheless, the autoresonant stage is bounded to the interval $-2 < |\alpha|\xi < 0$, as compared to $-2 < |\alpha|\xi < 4$ for $\alpha > 0$. In addition, the initial phase locking stage in the $\alpha < 0$ case settles at the average value of $\Phi \approx \pi$, in contrast to $\Phi \approx 0$ for $\alpha > 0$.

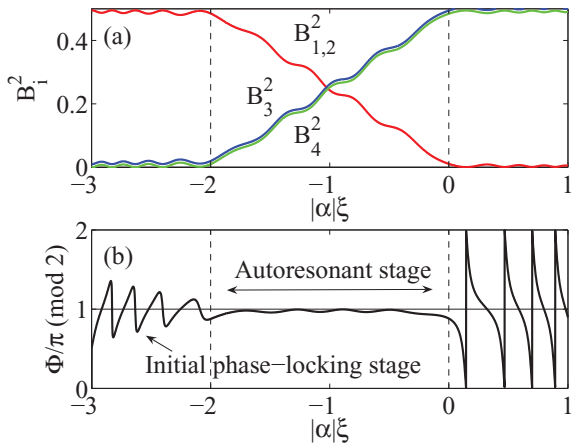

FIG. 2. (Color online) Autoresonant evolution of (a) wave envelopes B_i^2 and (b) phase mismatch Φ in a tapered fiber OPA versus normalized distance $|\alpha|\xi$ along the fiber for negative spatial chirp rate, $\alpha = -0.06$. The equal pumps $B_{1,2}^2$ are shown by the red (decreasing) curve, the signal B_3^2 is shown by the blue (upper increasing) curve and the idler B_4^2 is shown by the green (lower increasing) curve. Note that the curves of the signal and the idler are almost overlapping.

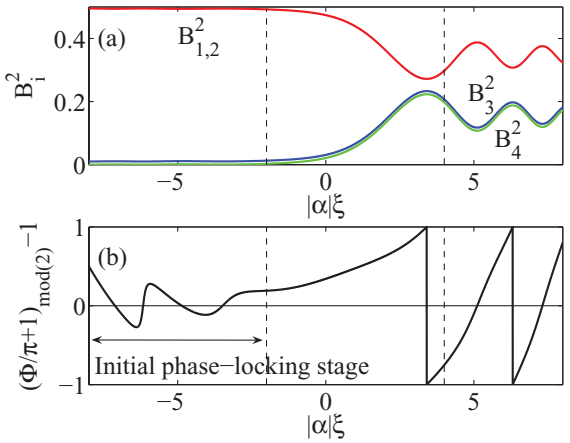

FIG. 3. (Color online) (a) Wave envelopes B_i^2 and (b) phase mismatch Φ versus normalized distance $|\alpha|\xi$ along the fiber. In this example all parameters are the same as in Fig. 1, but chirp rate $\alpha = 2$ is too large for entering the autoresonant regime. The pump depletion is not complete in this case. The equal pumps $B_{1,2}^2$ are shown by the red (decreasing) curve, the signal B_3^2 is shown by the blue (upper increasing) curve and the idler B_4^2 is shown by the green (lower increasing) curve. Note that the curves of the signal and the idler are almost overlapping.

Finally, Fig. 3 presents an example with higher value of $\alpha = 2$. One can see in the figure that the autoresonant stage is absent, although the initial phase-locking does occur.

The next section presents the theory of the dynamics illustrated in the numerical examples in Figs. 1–3.

III. AUTORESONANT DYNAMICS OF TAPERED FIBER OPA

A. Initial phase-locking and evolution of the signal-idler waves

In seeking most efficient autoresonant interaction (full depletion of the pumps), we assume that the initial normalized amplitudes of the pump waves are equal, $B_{10} = B_{20} = B_0$. We start at sufficiently large negative linear dephasing $|\alpha|\xi_{\mathrm{in}}$ and assume that the initial signal is small, $B_{30} \ll B_0$, and that $B_4(z) \ll B_3$ in the initial stage, since the idler is excited from zero. Consequently, we neglect the variation of B_3 and the depletion of the pump waves at this stage and focus on the evolution of B_4. Then, $Q \approx B_{30}/B_4$ and one can neglect the nonlinear term $-4B_4^2$ in Eq. (10) for Φ, yielding the approximation

$$\frac{dB_4}{d\xi} = B_{30}\sin\Phi, \quad \frac{d\Phi}{d\xi} = \alpha\xi + \frac{B_{30}}{B_4}\cos\Phi, \tag{11}$$

where we used $B_0 \approx 1/2$ due to our normalization $\sum_{l=1}^{4} B_l^2 = 1$. Equations (11) can be combined into a single complex equation for a new variable $Z = B_4 \exp(i\Phi)$:

$$\frac{dZ}{d\xi} = i\alpha\xi Z + iB_{30}. \tag{12}$$

The general solution of this equations is a sum of the general solution of the homogeneous problem for Z and a particular solution of the inhomogeneous problem:

$$Z = A\exp(i\alpha\xi^2/2) + B(\xi).$$

Here, we will use the asymptotic (at large $|\xi|$) slow inhomogeneous solution $B(\xi) \approx -B_{30}/(\alpha\xi)$. Finally, the constant A is obtained from the initial condition $[Z(\xi_{\text{in}}) = 0]$, yielding the idler wave in the initial excitation stage:

$$Z = \frac{B_{30}}{\alpha\xi_{\text{in}}}\left[e^{i\alpha(\xi^2-\xi_{\text{in}}^2)/2} - \frac{\xi_{\text{in}}}{\xi}\right].$$

This solution shows that as $|\xi|$ decreases and ξ_{in}/ξ becomes large, Z approaches $-B_{30}/(\alpha\xi)$, i.e., our system phase-locks at either $\Phi \approx 0$ or $\Phi \approx \pi$ for α positive or negative, respectively. One can see this adiabatic initial phase-locking transition in the numerical examples in Figs. 1 and 2. At the same time B_4 grows as $|Z| \approx B_{30}/|\alpha\xi|$ and, at some point, one must also include the corresponding growth of the signal wave. Nevertheless, we can still neglect the depletion of the pump waves as long as $B_{3,4} \ll B_0$. This problem is discussed next.

The combined signal-idler wave problem in the initial phase-locking stage is described by the approximate system

$$\frac{dB_4}{d\xi} = B_3 \sin\Phi,\ B_3^2 = B_{30}^2 + B_4^2, \tag{13}$$

$$\frac{d\Phi}{d\xi} = \alpha\xi + \left(\frac{B_4}{B_3} + \frac{B_3}{B_4}\right)\cos\Phi. \tag{14}$$

We have shown above that initially in this problem, Φ is already efficiently locked near zero or π, depending on the sign of α. We will show now that for sufficiently small α, this phase locking continuous, i.e., the solution stays close to the phase-locked quasisteady state solution $\widehat{B}_{3,4}$, $\widehat{\Phi}$ of the extended system satisfying

$$\alpha\xi + \left(\frac{\widehat{B}_4}{\widehat{B}_3} + \frac{\widehat{B}_3}{\widehat{B}_4}\right)\cos\widehat{\Phi} = 0, \tag{15}$$

$$\sin\widehat{\Phi} = \frac{1}{\widehat{B}_3}\frac{d\widehat{B}_4}{d\xi}. \tag{16}$$

First, we prove the existence of this solution and later, in Sec. III C, discuss its stability. Assuming $\widehat{\Phi} \ll 1$ for $\alpha > 0$ (or $|\widehat{\Phi} - \pi| \ll 1$ for $\alpha < 0$), we can approximate Eq. (15) as $|\alpha|\xi + q + 1/q \approx 0$, where $q = \widehat{B}_4/\widehat{B}_3$. This equation yields monotonically growing solution

$$q = \frac{|\alpha\xi|}{2} - \sqrt{\frac{(\alpha\xi)^2}{4} - 1}$$

scaling as $q = 1/|\alpha\xi|$ at large $|\alpha\xi|$ and approaching $q = 1$ at $|\alpha\xi| \to 2$. At this point, we test our assumption of smallness of $\widehat{\Phi}$. By definition, $dq/d\xi = (1-q^2)\sin\widehat{\Phi}$. On the other hand, for negative ξ, $\frac{dq}{d\xi} = \frac{|\alpha|q^2}{1-q^2}$. Then, $\sin\widehat{\Phi} = |\alpha|q^2/(1-q^2)^2$. This relation shows that our $|\cos\widehat{\Phi}| \approx 1$ approximation holds for $|\alpha|$ sufficiently small even as q approaches unity. For example, setting $\sin\widehat{\Phi} = 0.5$ as the limit of our $\cos\widehat{\Phi} \approx 1$ approximation, q can reach 0.85 within this approximation, if $|\alpha| < 0.053$. However, as q and, thus, $\widehat{B}_{3,4}$ continue to increase ($|\alpha|\xi \to -2$), $\widehat{\Phi}$ becomes large and our approximate quasisteady state solution becomes invalid. Nevertheless, if, at this stage, we include all the neglected nonlinear terms in Eq. (10) and take into account the depletion of the pump waves beyond $|\alpha|\xi = -2$, the quasisteady state locked at $\widehat{\Phi} \approx 0$ or π (depending on the sign of α) continues, as the wave amplitudes adjust themselves automatically, until one reaches nearly complete pump depletion. This phase-locked (autoresonant) quasisteady state beyond $|\alpha|\xi = -2$ is discussed next.

B. Autoresonant quasisteady state

In the region $|\alpha|\xi > -2$ we again assume $|\cos\Phi| \approx 1$, and set $B_4/B_3 \approx 1$, as discussed above, while $B_1/B_2 = 1$ due to our initial conditions. We define the autoresonant quasisteady state via [compare to Eqs. (15), (16)]

$$\alpha\xi - 4\widehat{B}_4^2 + s\widehat{Q} = 0, \tag{17}$$

$$\sin\widehat{\Phi} = \frac{1}{2\widehat{B}_1^2\widehat{B}_4}\frac{d\widehat{B}_4}{d\xi}, \tag{18}$$

where $\widehat{Q} = 2\widehat{B}_1^2\widehat{B}_3\widehat{B}_4(\widehat{B}_3^{-2} + \widehat{B}_4^{-2} - 2\widehat{B}_1^{-2}) \approx 4(\widehat{B}_1^2 - \widehat{B}_4^2) \approx 2 - 8\widehat{B}_4^2$, and $s = \text{sign}(\alpha)$. Then, from Eq. (17) we find

$$\widehat{B}_4^2 = \begin{cases} \frac{1}{12}(|\alpha|\xi + 2), \alpha > 0,\ -2 < |\alpha|\xi < 4, \\ \frac{1}{4}(|\alpha|\xi + 2), \alpha < 0,\ -2 < |\alpha|\xi < 0, \end{cases} \tag{19}$$

while from the Manley-Rowe relation

$$\widehat{B}_1^2 = \begin{cases} \frac{1}{12}(4 - |\alpha|\xi), \alpha > 0,\ -2 < |\alpha|\xi < 4, \\ -\frac{1}{4}|\alpha|\xi, \alpha < 0,\ -2 < |\alpha|\xi < 0. \end{cases} \tag{20}$$

The upper bounds on $|\alpha|\xi$ in these autoresonant steady states correspond to the locations of full pump depletion, $\widehat{B}_1^2 = 0 (\widehat{B}_4^2 = 1/2)$. The predicted linear averaged dependence of $B_{1,4}^2$ in the corresponding regions of $|\alpha|\xi$ is seen in our numerical examples in Figs. 1 and 2. Using Eqs. (19) and (20) we find from Eq. (18) that $\widehat{\Phi}$ is continuously small for sufficiently small $|\alpha|$, unless one approaches the limiting values of $|\alpha|\xi$, where our autoresonant solutions become invalid. Transition through these limiting values requires a special attention and will be discussed in the next subsection.

C. Stability of phase-locked solutions

We have already discussed the quasisteady state solutions in the tapered fiber OPA and showed that the system approaches these quasisteady states in the initial phase locking stage ($|\alpha|\xi < -2$). Here, we will show that this initial approach is sufficient for continuing autoresonance in the system, i.e., prove that the quasisteady state solutions are stable for $|\alpha|$ small enough. In studying the stability, we assume solution close to the steady state, i.e., write $B_4 = \widehat{B}_4 + \delta$, where δ is small, replace $\cos\Phi$ in Eqs. (10) by $s = \text{sign}(\alpha)$ and expand this equation to first order in δ, yielding

$$\frac{d\Phi}{d\xi} = (\alpha\xi - G) - sG'\delta, \tag{21}$$

where $G = 4\widehat{B}_4^2 - s\widehat{Q}$, where $\widehat{Q}$ is $2B_1^2B_3B_4(B_3^{-2} + B_4^{-2} - 2B_1^{-2})$ evaluated at $\widehat{B}_4$. Next, we define $\widehat{B}_4$ in our system at all stages of evolution (including the initial phase-locking

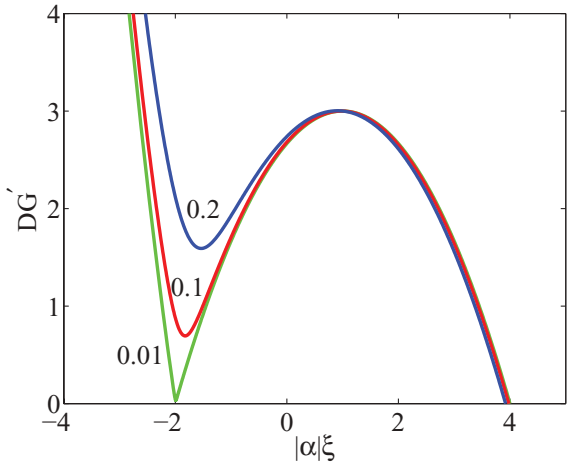

FIG. 4. (Color online) Stability function DG' versus $|\alpha|\xi$ for $\alpha > 0$ and different values of initial signal amplitude B_{30}. $DG' \gg |\alpha|$ is required for continuing autoresonance in the system. $B_{30} = 0.2$ for the upper blue curve, $B_{30} = 0.1$ for the intermediate red curve and $B_{30} = 0.01$ for the lower green curve.

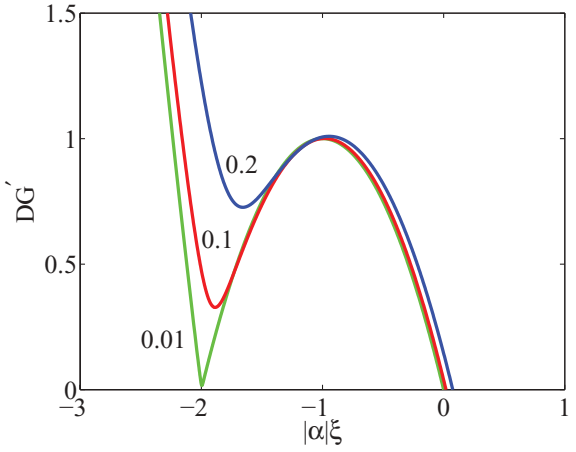

FIG. 5. (Color online) Stability function DG' versus $|\alpha|\xi$ for $\alpha < 0$ and different values of initial signal amplitude B_{30}. $DG' \gg |\alpha|$ is required for continuing autoresonance in the system. $B_{30} = 0.2$ for the upper blue curve, $B_{30} = 0.1$ for the intermediate red curve and $B_{30} = 0.01$ for the lower green curve.

stage $|\alpha|\xi < -2$, the autoresonant stage $|\alpha|\xi > -2$, and the transition region $|\alpha|\xi \approx -2$ between the two stages) via

$$G \equiv \alpha\xi. \tag{22}$$

Then,

$$\frac{d\Phi}{d\xi} = -sG'\delta. \tag{23}$$

On the other hand, $d\delta/d\xi = dB_4/d\xi - d\widehat{B}_4/d\xi$, which, using Eq. (9) to lowest order in δ and $d\widehat{B}_4/d\xi = \alpha/G'$ obtained by differentiation of Eq. (22), yields

$$\frac{d\delta}{d\xi} = sD\sin\Phi - \alpha/G', \tag{24}$$

where $D = 2\widehat{B}_1\widehat{B}_2\widehat{B}_3$ and $\sin\Phi$ was replaced by $s\sin\Phi$ (equivalent to shifting Φ by π in the case of negative α). One observes that Eqs. (23) and (24) are Hamilton equations for canonical variables δ and Φ governed by Hamiltonian

$$H(\delta,\Phi,\xi) = -\frac{sG'}{2}\delta^2 + V_{\text{eff}}(\Phi,\xi),$$

where $V_{\text{eff}} = sD\cos\Phi + \alpha\Phi/G'$ and ξ plays a role of "time." Note that V_{eff} is a tilted "washboard" potential with slow "time"-dependent parameters D and G'. Thus, our quasisteady states are stable, as long as the effective potential has well defined minima, i.e.,

$$|\alpha| \ll DG', \tag{25}$$

which is the desired stability condition. We present the dependence of DG' on $|\alpha|\xi$ in Figs. 4 and 5 for different values of the initial amplitude of the signal. The figures show that the quasisteady states are stable for the value of $|\alpha|$ in the examples in Figs. 1 and 2 and unstable for the case illustrated in Fig. 3. Note also that stable evolution of the system involves small spatial modulations around the slowly evolving quasisteady states. These modulations are seen in the examples in Figs. 1 and 2 and have characteristic "frequency" $\Omega \approx \sqrt{DG'}$. Therefore, condition (25) can be written as $|\alpha| \ll \Omega^2$. A simple expression for Ω can be obtained in the autoresonant regime, where $D \approx (4 - |\alpha|\xi)(|\alpha|\xi + 2)^{1/2}/(12\sqrt{3})$, $|G'| \approx 12(2 + |\alpha|\xi)^{1/2}/\sqrt{3}$, so $\Omega^2 \approx (4 - |\alpha|\xi)(|\alpha|\xi + 2)/3$ for $\alpha > 0$, and $D \approx -|\alpha|\xi(|\alpha|\xi + 2)^{1/2}/4$, $|G'| \approx 4(|\alpha|\xi + 2)^{1/2}$, so $\Omega^2 \approx -|\alpha|\xi(|\alpha|\xi + 2)$ for $\alpha < 0$. Note that the most stringent condition on $|\alpha|$ corresponds to the transition between the initial phase locking and autoresonant stages, i.e., at $|\alpha|\xi \approx -2$, while after entering the autoresonant stage, $|\alpha|$ can be increased without loosing stability. This conclusion has practical consequences, allowing to decrease the tapered fiber length still preserving autoresonance and reaching complete pump depletion. Note also that when the pumps are depleted near $|\alpha|\xi \approx 4$ or 0 for α positive or negative, respectively, Figs. 4 and 5 show that the stability condition (25) is violated, and the autoresonant phase-locking discontinues.

D. Implementation of the theory

Our theory above presented analysis of autoresonant four-wave mixing using dimensionless variables and parameters for a single set of pump/signal frequencies. Here, we apply the theory in an example of a realizable tapered fiber and calculate the spectral band of the associated autoresonant OPA. The technology of fabricating tapered fibers has advanced in the past decade and currently tapered fibers of a wide range of lengths (from less than 10 cm up to more than 10 m) are available [14]. Our numerical example below will correspond to a step-index fiber of length $L = 10$ m with a linearly varying core radius between $a_{\text{in}} = 2.3\,\mu$m and $a_f = 2.2\,\mu$m. The cladding radius is much larger than the core radius and will be assumed to be infinite in the our analysis. We use two pumps of frequency $f_1 = \omega_1/(2\pi) = 160$ THz and $f_2 = \omega_2/(2\pi) = 208$ THz (corresponding to wavelengths $\lambda_1 = 1.87\,\mu$m and $\lambda_2 = 1.44\,\mu$m in a vacuum). The pump waves have equal power of 1 kW and the signal has a power of 20 W. Such pump powers may be obtained by using pulsed lasers. If the pulse length is much longer than L/c, transient effects are negligible at times $t \gg L/c = 33$ nsec and we may

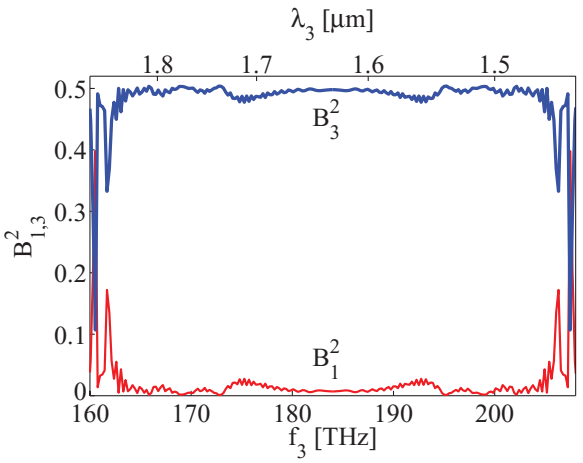

FIG. 6. (Color online) The amplification spectrum of the autoresonant OPA. The normalized intensity of the signal, B_3^2 (blue upper line), and the pump, B_1^2 (red lower line), versus the signal frequency f_3 and wavelength λ_3.

use a CW theory. Although these 1 kW pumps yield a relatively high average intensity of the order of 133 $\mathrm{W}/\mu\mathrm{m}^2$, this value is significantly lower than the damage threshold of fused silica, which is 4750 $\mathrm{W}/\mu\mathrm{m}^2$ [15].

At this stage we relate the spatial chirp rate α and the reduced coordinate ξ in our model [see (9) and (10)] to our fiber parameters:

$$\alpha = \frac{1}{(\gamma_{\mathrm{avg}} P_0)^2}\left(\frac{\Delta\beta_f - \Delta\beta_{\mathrm{in}}}{L}\right), \tag{26}$$

$$\xi = \frac{1}{\alpha}\left(\frac{\Delta P_0}{P_0} + \frac{\Delta\beta}{\gamma_{\mathrm{avg}} P_0}\right). \tag{27}$$

Here, we assume linear tapering, $\Delta\beta_f$ and $\Delta\beta_{\mathrm{in}}$ are the values of $\Delta\beta$ at the final and initial radii of the fiber, γ_{avg} is a characteristic value of the nonlinearity coefficient along the fiber, and L is its length. We discuss the dependence of $\Delta\beta$ on fiber parameters and frequencies of the interacting waves in detail in the Appendix. The Appendix shows that, importantly, for a given pair of pump frequencies $\omega_{1,2}$, the tapered fiber radius in our OPA must be close to the "zero dispersion" radius a_0. The latter is defined as the radius at which the second order derivative $\beta_2^c = \partial^2\beta/\partial\omega^2$ of the propagation constant of the fiber evaluated at the central pump frequency $\omega_c = (\omega_1 + \omega_2)/2$ vanishes. Then, see Eq. (A9),

$$d\Delta\beta/da \approx \frac{1}{192}\frac{\partial\beta_4^c}{\partial a_0}[(2\omega_3 - \omega_1 - \omega_2)^4 - (\omega_1 - \omega_2)^4],$$

and, therefore,

$$\alpha \approx \frac{1}{192}\frac{\partial\beta_4^c}{\partial a_0}\frac{(a_f - a_{\mathrm{in}})}{(\gamma P_0)^2 L}[(2\omega_3 - \omega_1 - \omega_2)^4 - (\omega_1 - \omega_2)^4]. \tag{28}$$

Note that the sign of α as a function of the signal frequency ω_3 changes as ω_3 passes one of the pump frequencies, $\omega_{1,2}$. These relations allow to use the theory developed above in calculating the spectral characteristics in our autoresonant OPA. Figure 6 shows the spectral amplification profile of the signal wave (blue upper line) from numerical simulations, using Eq. (26) versus the frequency $f_3 = \omega_3/(2\pi)$ for the parameters listed above. We observe that the spectrum is symmetric with respect to f_3 [reflecting the same symmetry in Eq. (28)] and nearly flat in a wide frequency band between the pump frequencies due to almost complete pump depletion (we show B_1^2 of the pump in the same figure by a red lower line). This is a consequence of the fact that for the chosen set of parameters, the chirp rate is small enough and the stability condition Eq. (25) is satisfied in an extended spatial region for all signal frequencies. The gain decrease near $f_1 = 160$ THz and $f_2 = 208$ THz is due to $\alpha \to 0$ at these frequencies, i.e., when the fiber is nearly uniform and of insufficient length for extended autoresonant interaction. This completes our discussion of autoresonant tapered fiber OPA.

IV. CONCLUSIONS

In conclusion:

(i) We have studied autoresonant four-wave mixing dynamics in a tapered fiber OPA. In autoresonance a continuous nonlinear phase-locking between two pump, signal, and idler waves is achieved via the self-adjustment of the wave amplitudes despite variation of system parameters (radius of the fiber) and without a need of feedback.

(ii) We have shown that a successful autoresonant interaction requires starting out and passage through resonance. The initial phase-locking in the system is achieved prior the passage through resonance and is later maintained if the spatial chirp rate α of the fiber is sufficiently small [see Eq. (25)]. The most stringent condition on the chirp rate exists at the end of the initial phase-locking stage, just prior the passage through resonance. Beyond this location, the chirp rate can be significantly increased allowing to shorten the length of the tapering required for reaching full pump depletion.

(iii) After the initial phase-locking stage the system enters autoresonant interaction stage, where the variation of the linear propagation constant of the fiber is automatically balanced by the nonlinear dispersion in the system. At this stage, one obtains a simple analytic dependence of the slow waves' envelopes on the distance z along the fiber. For example, for a constant chirp rate α, the powers of all interacting waves vary linearly with z, and the signal and idler fluxes increase, until a nearly complete pumps depletion is achieved for a sufficient length of the fiber (see examples in Figs. 1 and 2).

(iv) The monotonic autoresonant growth of the signal and idler powers in the tapered fiber at the expense of the pumps is accompanied by small characteristic oscillating modulations of the powers. These modulations manifest stability of the underlying nonlinear resonance in the slowly varying system. Because of this stability, the autoresonant phase-matching and the resulting amplification of the signal wave along the tapered fiber is not sensitive to the exact form of the tapering, as long as this tapering is sufficiently slow. Furthermore, the autoresonant amplification is not affected by sufficiently adiabatic spatial fiber imperfections.

(v) Efficient amplification (complete pump depletion) in the autoresonant OPA can be achieved for both positive and negative spatial chirp rates of the fiber. In addition, because of the automatic phase-locking in the amplifier, it yields a wide and nearly flat spectral band for efficient amplification (see

example in Fig. 6). The spectral width of the flat amplification profile is limited by the length of the tapered fiber.

(vi) In purpose to limit the length of the fiber in the examples presented in this work to ten meters, we used 1 kW powers of the pumps. These powers are not suitable for CW operation of the amplifier in communication applications, but may be utilized in pulsed applications, such as laser frequency conversion, for example. Furthermore, at high powers of the pump waves, other nonlinear processes, such as Raman and Brillouin scattering may become important. The study of these effects on autoresonance in the system was outside the scope of this work and comprise an important goal for future research. Finally, all our examples used conventional, weakly guiding fibers with total of about 5% tapering of the core radius and assumed near constancy of the nonlinearity parameter along the fiber. It is important to extend the theory to tapered fibers with air cladding, which may reduce the fiber length required for efficient operation of the amplifier.

ACKNOWLEDGMENTS

This work was supported by the Israel Science Foundation Grant No. 294/05.

APPENDIX: FIBER PARAMETERS

1. Refractive index

We will assume that the refractive indices n of both the core and the cladding are given by the Sellemeier equation:

$$n^2(\lambda) = 1 + \sum_{j=1}^{3} \frac{a_j \lambda^2}{\lambda^2 - l_j^2}, \tag{A1}$$

where a_j, l_j are material parameters. The dispersion relation in a uniform material is

$$\omega - \frac{2\pi c}{\lambda n(\lambda)} = 0. \tag{A2}$$

The cladding in our examples is fused silica without doping for which [16]: $a_1 = 0.696\,166\,30$, $a_2 = 0.407\,942\,60$, $a_3 = 0.897\,479\,40$, $l_1 = 0.068\,404\,300$, $l_2 = 0.116\,241\,40$, $l_3 = 9.896\,161\,0$. The formula is valid in the range $0.21\,\mu\text{m} < \lambda < 3.71\,\mu\text{m}$. The core material is doped silica (P 12.5 wt%, Cl 0.03 wt%) with parameters [17]: $a_1 = 0.515\,12$, $a_2 = 0.628\,04$, $a_3 = 1.074\,3$, $l_1 = 0.026\,36$, $l_2 = 0.116\,14$, $l_3 = 10.693\,1$.

2. Propagation constant and nonlinearity coefficient

Following Ref. [18], we calculate the propagation factor β versus the core radius as follows. If k is the wave number in free space and n_{co}, n_{cl} are the refractive indices of the core and cladding, respectively, then $n_{cl}k \leqslant \beta \leqslant n_{co}k$. Define

$$V = ak\left(n_{co}^2 - n_{cl}^2\right)^{\frac{1}{2}}, \tag{A3}$$

and assume that the relative difference $\Delta = (n_{co} - n_{cl})/n_{cl}$ between the refractive indices of the core and the cladding is small (weak guiding). In most optical fiber applications, the value of Δ does not exceed 0.003 to avoid high losses while propagating in fiber bendings [19]. However, since our fiber is straight and short this constraint is irrelevant and we will let Δ reach values of up to 0.01. We will also assume a single HE_{11} mode operation. This requires that $V < 2.405$ everywhere within the tapered fiber, condition satisfied in all our numerical examples. For the HE_{11} mode one finds [18]

$$\beta(V) = nk\,(1 + \Delta[1 - \chi^2]), \tag{A4}$$

where $\chi = (1 + \sqrt{2})/[1 + (4 + V)^{\frac{1}{4}}]$. Furthermore, the nonlinear coefficient γ is defined as $\gamma(\omega) = k(\omega)n_2(\omega)/A_{\text{eff}}$, where n_2 is nonlinear refractive index and A_{eff} is the effective mode area [3]. Approximating the transverse mode profile by a Gaussian of width w yields $A_{\text{eff}} = \pi w^2$. Since the mode radius can be related to V as $w = a/\sqrt{\ln V}$ (assuming that $V > 1$, which is valid in our examples), the nonlinearity coefficient is given by [3]

$$\gamma = \frac{2n_2 \ln V}{\lambda a^2}. \tag{A5}$$

Choosing a typical value of $n_2 = 2.4 \times 10^{-20}$ m^2/W [3] and recalling that in our numerical examples $2.2\,\mu\text{m} < a < 2.3\,\mu\text{m}$, we find that $3(\text{Wkm})^{-1} < \gamma < 5.6(\text{Wkm})^{-1}$. For simplicity, throughout this work, we assume that γ is constant and equal to $\gamma_{\text{avg}} = 4.3(\text{Wkm})^{-1}$.

3. Mismatch $\Delta\beta$

We assume the resonance condition $\omega_1 + \omega_2 = \omega_3 + \omega_4$ in our two pump OPA system. The mismatch $\Delta\beta$ is defined as

$$\Delta\beta = \beta_3 + \beta_4 - \beta_1 - \beta_2 = \beta(\omega_3) + \beta(\omega_4) - \beta(\omega_1) - \beta(\omega_2). \tag{A6}$$

Due to the resonance condition in the OPA, for given pump frequencies ω_1, ω_2, $\Delta\beta$ can be viewed as dependent on the signal frequency ω_3 and the slowly varying core radius $a(z)$ only. We expand $\Delta\beta$ around the central pump frequency $\omega_c = (\omega_1 + \omega_2)/2$ [3]:

$$\Delta\beta(\omega_3, a) = 2\sum_{m=1}^{\infty} \frac{\beta_{2m}^c(a)}{(2m)!}\left(\Delta\omega_s^{2m} - \omega_d^{2m}\right), \tag{A7}$$

where $\Delta\omega_s \equiv (\omega_3 - \omega_c)$, $\omega_d = (\omega_1 - \omega_2)/2$, and $\beta_{2m}^c \equiv \partial^{2m}\beta/\partial\omega^{2m}$ is evaluated at $\omega = \omega_c$. Denoting by a_0 the core radius for which β_2^c vanishes, and assuming that both $\Delta\omega_s$ and ω_d are sufficiently small, upon expansion of $\beta_{2m}^c(a)$ around a_0, to lowest order we obtain

$$\Delta\beta(\omega_3, a) \approx \frac{\beta_{40}^c + \beta_{40}^{c\prime}(a - a_0)}{12}\left(\Delta\omega_s^4 - \omega_d^4\right), \tag{A8}$$

where β_{40}^c and $\beta_{40}^{c\prime}$ are $\beta_4^c(a)$ and its derivative evaluated at a_0. Here, we substitute the assumed linear variation of the core radius along the fiber $a(z) = a_{\text{in}} + (a_f - a_{\text{in}})z/L$ to get

$$\Delta\beta(z) = \tilde{\alpha}(z - z_0),$$

where z_0 is the point at which $\Delta\beta$ vanishes and the spatial fiber chirp rate is

$$\tilde{\alpha} = \frac{(a_f - a_{\text{in}})\beta_{40}^{c\prime}}{192L}[(2\omega_3 - \omega_1 - \omega_2)^4 - (\omega_1 - \omega_2)^4]. \tag{A9}$$

[1] E. R. Tracy, A. N. Kaufman, and A. J. Brizard, Phys. Plasmas **10**, 2147 (2003).
[2] D. J. Kaup, A. Rieman, and A. Bers, Rev. Mod. Phys. **51**, 275 (1979).
[3] G. P. Agrawal, *Nonlinear Fiber Optics* (Elsevier Inc., New York, 2007).
[4] E. M. Marhic, *Fiber Optical Parametric Amplifiers, Oscilltors and Related Devices* (Cambridge University Press, Cambridge, 2008).
[5] V. Veksler, J. Phys. USSR **9**, 153 (1945).
[6] E. M. McMillan, Phys. Rev. **68**, 143 (1945).
[7] J. Fajans and L. Friedland, Am. J. Phys. **69**, 1096 (2001).
[8] L. Friedland, Scholarpedia **4**, 5473 (2009).
[9] L. Friedland, Phys. Fluids B **4**, 3199 (1992).
[10] L. Friedland, Phys. Rev. Lett. **69**, 1749 (1992).
[11] O. Yaakobi, L. Friedland, R. R. Lindberg, A. E. Charman, G. Penn, and J. S. Wurtele, Phys. Plasmas **15**, 032105 (2008).
[12] O. Yaakobi and L. Friedland, Phys. Plasmas **15**, 102104 (2008).
[13] A. Barak, Y. Lamhot, L. Friedland, and M. Segev, Phys. Rev. Lett. **103**, 123901 (2009).
[14] N. Vukovic, N. G. R. Broderick, M. Petrovich, and G. Brambilla, IEEE Photonics Technol. Lett. **20**, 1264 (2008).
[15] A. V. Smith, B. T. Do, G. R. Hadley, and R. L. Farrow, IEEE J. Sel. Top. Quantum Electron. **15**, 153 (2009).
[16] I. H. Malitson, J. Opt. Soc. Am. A **55**, 1205 (1965).
[17] O. V. Butov, K. M. Golanta, A. L. Tomashuk, M. J. N. van Stralen, and A. H. E. Breuls, Opt. Commun. **213**, 301 (2002).
[18] D. Gloge, Appl. Opt. **10**, 2252 (1971).
[19] D. Gloge, IEEE Trans. Microwave Theory Tech. **23**, 106 (1975).